Solid Earth Discuss., https://doi.org/10.5194/se-2017-86
Manuscript under review for journal Solid Earth
Discussion started: 29 August 2017

Solid Earth Discussions
Open Access
EGU

Variability of geothermal gradient across two differently aged continental volcanic passive margins: The Southwest African and the Norwegian margins

Ershad Gholamrezaie[1,2], Magdalena Scheck-Wenderoth[2,3], Judith Sippel[2], and Manfred R. Strecker[1]

[1]Institute of Earth and Environmental Science, University of Potsdam, Germany
[2]Helmholtz Centre Potsdam–GFZ German Research Centre for Geosciences, Postdam, Germany
[3]Faculty of Georesources and Material Engineering, RWTH Aachen, Aachen, Germany

Correspondence to: Ershad Gholamrezaie (ershad@gfz-potsdam.de)

Abstract. The aim of this study is to investigate the shallow thermal field differences for two differently aged passive continental margins by analyzing regional variations in geothermal gradient and exploring the controlling factors for these variations. Hence, we analyzed two previously published 3D conductive and lithospheric-scale thermal models of the Southwest African and the Norwegian passive margins. These 3D models differentiate various sedimentary, crustal and mantle units and integrate different geophysical data such as seismic observations and the gravity field. We extracted the temperature-depth distributions in 1 km intervals down to 6 km below the upper thermal boundary condition. The geothermal gradient was then calculated for these intervals between the upper thermal boundary condition and the respective depth levels (1, 2, 3, 4, 5, and 6 km below the upper thermal boundary condition). According to our results, the geothermal gradient decreases with increasing depth and shows varying lateral trends and values for these two different margins. We compare the 3D geological structural models and the geothermal gradient variations for both thermal models and show how radiogenic heat production, sediment insulating effect, and thermal LAB depth influence the shallow thermal field pattern. The results indicate an ongoing process of oceanic mantle cooling at the young Norwegian margin compared with the old SW African passive margin that seems to be thermally equilibrated at the present-day.

1 Introduction

Comprehension of the lithosphere-scale thermal state is a key to unraveling the evolution, strength, and physical and chemical processes of the lithosphere (e.g., Artemieva and Mooney, 2001; Chapman, 1986; McKenzie et al., 2005; Davies, 1980; Scheck-Wenderoth and Lamarche, 2005; Ebbing et al., 2009). Furthermore, analyzing the thermal field of the lithosphere has important applications in industrial sectors such as geo-resources exploration (e.g., Tissot et al., 1987; Muffler and Cataldi, 1978; Grevemeyer and Villinger, 2001; Wallmann et al., 2012).

The lithospheric thermal field generally depends on the thermal thickness and the thermal properties of the lithosphere (Turcotte and Schubert, 2014; Scheck-Wenderoth and Maystrenko, 2008; Artemieva, 2006). There is a consensus that conduction is the main heat transfer mechanism in the lithosphere and generally controlled by (1) the heat input from larger mantle depths,

Solid Earth Discuss., https://doi.org/10.5194/se-2017-86
Manuscript under review for journal Solid Earth
Discussion started: 29 August 2017

(2) the heat internally produced in the lithosphere by the decay of radioactive elements, and (3) the thermal conductivity of different lithospheric layers (Turcotte and Schubert, 2014; Allen and Allen, 2005). The interaction of these controlling factors complicates predictions of temperature increase with depth. This difficulty largely arises from the variability of the lithosphere in terms of structure and composition, parameters that are a product of the tectonic setting and evolution of the location of interest. One well-established strategy to investigate the present-day thermal field of a certain area is to integrate existing geophysical and geological data into 3D structural models that provide the basis for numerical modeling, which simulates heat transport processes after setting boundary conditions and thermal properties according to the geological structure (e.g., Scheck-Wenderoth and Lamarche, 2005; Noack et al., 2013; Scheck-Wenderoth et al., 2014; Sippel et al., 2015; Balling et al., 2016).

Although there is already a large number of such 3D models for different settings worldwide, none of these studies has focused on the variability of geothermal gradients with respect to geological structure. It is self-evident that the geothermal gradient is a function of local temperature, which depends on the thermal state. This is an important issue, because, geothermal gradient variations in the shallow parts of the subsurface (measured or modeled) may be indicative of the thermal field and temperature-controlled processes at greater depths. Moreover, methods used to assess the thermal history of specific tectonic settings generally apply strongly simplified assumptions concerning the geothermal gradient and its changes in space and time (e.g., Allen and Allen, 2005; Naeser and McCulloh, 2012; Burnham and Sweeney, 1989; Barker, 1996). Accordingly, a better understanding of variations of the geothermal gradient could also improve the quality of thermochronological results of thermal history models. In this interest, the main questions are: (1) how does the geothermal gradient vary with depth and laterally over major geological structure (such as passive continental margins)?; (2) what are the controlling factors of these variations?; and (3) how are shallow geothermal gradients related to the lithospheric-scale thermal field?

The goal of this study is to investigate geothermal gradient as one manifestation of the thermal field that can directly be observed and usually differs significantly according to the specific tectonic settings. Our approach follows three principal steps: (1) derive geothermal gradients from two existing and validated 3D thermal models, both from volcanic passive margins, but with major age differences: the SW African passive margin (130 Ma) and the Norwegian margin (55 Ma); (2) investigate the variability of geothermal gradients with respect to the structural configuration changing from unthinned continental lithosphere onshore, over the stretched margins with great sediment thickness, and finally to the distal oceanic lithosphere; and (3) compare the results of the calculated geothermal gradients for the two different margins. In this context, there are significant variations in the thermal field that need to be considered, when sediments, crust, and the lithospheric mantle display pronounced lateral heterogeneities in thickness and composition across the continental margins. In spite of a very similar configuration of the crust, the underlying lithospheric mantle in the two study areas differs. The younger lithospheric mantle beneath the oceanic crustal parts of the North Atlantic is significantly thinner than the older counterpart of the South Atlantic (Scheck-Wenderoth et al., 2007; Scheck-Wenderoth and Maystrenko, 2008; Maystrenko et al., 2013). By comparing the calculated geothermal gradients of these margins, we particularly address the consequences of the lateral heterogeneities for the thermal field, and test the hypothesis that the present-day thermal field is different for the two settings and ultimately determined by the lithospheric mantle characteristics.

Solid Earth Discuss., https://doi.org/10.5194/se-2017-86
Manuscript under review for journal Solid Earth
Discussion started: 29 August 2017

Solid Earth Discussions
Open Access
EGU

Table 1. Oceanic lithosphere age after Müller et al. (2008) and average physical properties of geological units used for thermal modeling after Scheck-Wenderoth and Maystrenko (2008); Maystrenko et al. (2013).

Geological units	SW African margin				Norwegian margin			
	Age	Maximum thickness [km]	Average thermal conductivity [W/mK]	Average heat production [μW/m³]	Age	Maximum thickness [km]	Average thermal conductivity [W/mK]	Average heat production [μW/m³]
Clastic sediments	Cenozoic	Walvis Basin = 3.6 Lüderitz Basin = 3 Orange Basin = 1.4	1.5	1	Cenozoic	Vøring Basin = 3.2 Møre Basin = 3.6	1.5	1
	Cretaceous	Walvis Basin= 5 Lüderitz Basin= 8 Orange Basin= 15	1.5	1	Cretaceous	Vøring Basin = 16 Møre Basin = 13	1.5	1
Upper crystalline crust	-	50	2.8	1.45	-	40	2.7	0.8
High density crust	-	-	2.7	0.95	-	-	2.6	0.5
High velocity bodyt	-	-	2.6	0.8	-	-	2.3	0.2
Oceanic crust	130 Ma b.p.	-	2.75	0.3	55 Ma b.p.	-	2.1	0.3
Lithospheric mantle ($600^{\circ}C \leq T \leq 1300^{\circ}C$)	-	135	3.95	0.03	-	110	3.95	0.03

Solid Earth Discuss., https://doi.org/10.5194/se-2017-86
Manuscript under review for journal Solid Earth
Discussion started: 29 August 2017

2 Method

2.1 3D Conductive Thermal Model

Theoretically, heat is transfered due to a temperature gradient and dependent on the thermal conductivity within the solid media. This statement is known as the law of heat conduction or Fourier's law [eq. 1], where λ stands for the thermal conductivity, and ∇T defines the premier temperature gradient;

$$\boldsymbol{q} = -\lambda \nabla T. \tag{1}$$

Considering Fourier's law (Eq.1) and assuming conductive heat transport as the main heat transfer mechanism, the heat flow equation can be derived on a lithospheric scale (Eq. 2). In these equations T and t represent temperature and time, respectively. The radiogenic heat production is shown by S and Δ is the Laplacian operator. The parameter ρ stands for density, c for the heat capacity and λ for the thermal conductivity.

$$\rho c \frac{\partial T}{\partial t} = -\lambda \Delta T + S \tag{2}$$

The two considered 3D conductive thermal models (Scheck-Wenderoth and Maystrenko, 2008; Maystrenko et al., 2013) were created as a numerical solution to Eq. 2 in the steady-state condition ($\frac{\partial T}{\partial t}$= 0) and by considering lithology-dependent thermal properties (Table 1).

2.2 Geothermal Gradient

The geothermal gradient is the temperature change with increasing depth [Eq. 3]. Through the 3D thermal models, the corresponding temperature to a certain depth is predicted which simplifies the geothermal gradient calculation. However, since the aim of this study is to compare the variations of the geothermal gradient in different geological settings, a comparable reference frame is required. Therefore, the upper thermal boundary in each thermal model was chosen as the reference surface. We extracted the temperature-depth distributions in 1 km homogeneous depth intervals down to 6 km below the upper thermal boundary surface (Fig. 1). To calculate the geothermal gradient (Eq. 3), we considered "T_j" and "z_j" respectively as the temperature and the elevation of a surface in the 3D thermal models for which the upper thermal boundary condition was assigned to (Fig. 4a and 7a). In our calculation, "z_i" was the corresponding depth for $i = 1, 2, 3, 4, 5, 6$ km below the upper thermal boundary condition, and "T_i" was the temperature distributions at the corresponding depth levels of "i"s (Fig. 1). The geothermal gradient was then calculated for these intervals as the temperature difference between the uppermost surface and the corresponding depth levels. Thus, the average geothermal gradient is determined for increasingly thicker intervals with increasing depths.

$$\frac{dT}{dz} = \frac{T_i - T_j}{z_i - z_j} \tag{3}$$

Solid Earth Discuss., https://doi.org/10.5194/se-2017-86
Manuscript under review for journal Solid Earth
Discussion started: 29 August 2017

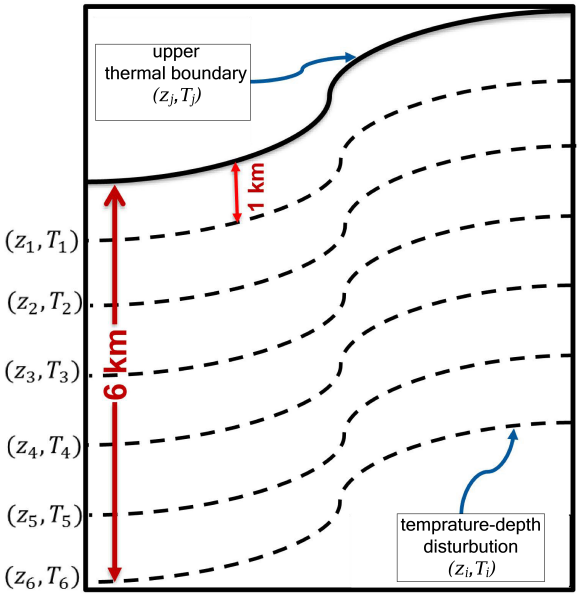

Figure 1. Schematic of the temperature-depth distributions in 1 km homogeneous depth intervals down to 6 km below the upper thermal boundary surface to calculate the geothermal gradient for specific depth intervals.

3 Exploited Models

The database for this study consists of regional 3D lithospheric-scale structural and thermal models for the SW African (Maystrenko et al., 2013) and the Norwegian passive margins (Scheck-Wenderoth et al., 2007; Scheck-Wenderoth and Maystrenko, 2008). These models integrate and are consistent with observed seismic data, gravity data, as well as with measured temperatures and heat flow.

3.1 Geological Background

Passive continental margins evolve in consequence to continental rifting and breakup with the formation of new oceanic crust (White et al., 1987). Rifted margins, according to the level of volcanism, are divided into two general categories: (a) magma-poor rifted margins and (b) volcanic rifted margins (Franke, 2013). One of the typical characteristics of volcanic passive margins is an extremely thinned continental crust ($\sim$ 5 km in the distal margin) that contains lower crustal bodies usually characterized by high p-wave velocities of more than 7.2 km/s (White et al., 1987; Talwani and Abreu, 2000; Franke, 2013). Two more characteristic features of volcanic passive margins are Seaward Dipping Reflectors (SDRs; interpreted as the expression of basaltic extrusions (Hinz, 1981; Mutter et al., 1982; White et al., 1987; White and McKenzie, 1989)), and usually more than 10 km thick syn- and post-rift sediments (White and McKenzie, 1989; Franke, 2013).

Solid Earth Discuss., https://doi.org/10.5194/se-2017-86
Manuscript under review for journal Solid Earth
Discussion started: 29 August 2017

The volcanic passive margin of Norway is the result of the last phase of Pangea breakup (55 Ma b.p) in the early Cenozoic. It evolved in response to the North Atlantic breakup, presumably, initiated by the abnormally hot mantle of the Iceland plume (White, 1989; Skogseid et al., 1992; Ren et al., 1998; Tsikalas et al., 2002; Blystad et al., 1995; Gernigon et al., 2004, 2006). The Norwegian continental margin records several pre-breakup rifting phases that played a major role in initiating the formation of deep sedimentary basins (Skogseid, 1994; Blystad et al., 1995; Swiecicki et al., 1998; Doré et al., 1999, 2002; Brekke, 2000; Skogseid et al., 2000). For instance, the deep Vøring and Møre basins in the Norwegian Sea were formed due to the early rifting around 150 Ma ago and contain more than 10 kilometers of late Mesozoic deposits (Scheck-Wenderoth et al., 2007).

In contrast, the causative breakup event leading to the creation of the South Atlantic and the formation of the SW African margin occurred significantly earlier than the Norwegian margin formation. About 130 Ma ago the continental lithosphere broke apart and generated the South Atlantic Ocean (Brown et al., 1995; Rabinowitz and LaBrecque, 1979; Nürnberg and Müller, 1991; O'Connor and Duncan, 1990; Unternehr et al., 1988; Larson and Ladd, 1973; Talwani and Abreu, 2000; Blaich et al., 2009). These processes were followed by rifting and post-breakup cooling, resulting in several sedimentary basins formed along the margins of the South Atlantic (Séranne and Anka, 2005; Macdonald et al., 2003; Stewart et al., 2000).

Both passive margin settings have similar configurations; crystalline crustal rocks crop out onshore, thick sedimentary sequences along the rifted margins are underlain by a severely thinned upper crust and are associated with high-velocity high-density lower crustal bodies, and display pronounced SDRs. The sedimentary units at both settings are predominantly composed of siliciclastic rocks with varying degrees of compaction (Stewart et al., 2000; Maystrenko et al., 2013; Scheck-Wenderoth et al., 2007; Scheck-Wenderoth and Maystrenko, 2008; Brekke, 2000).

3.2 Southwest African Passive Margin

There are three main sedimentary basins in the study area of the SW African continental margin. From North to South there are the Walvis Basin, the Lüderitz Basin, and the Orange Basin. These basins overlie a thinned continental crust and are filled with Cretaceous and Cenozoic sediments (Fig. 2a, Table 1). The Orange Basin hosts the thickest sediments compared to the two other basins with a maximum thickness of up to 16 km in the southern part of the basin. Sediment thickness varies in a similar manner in the Lüderitz and Walvis basins and ranges between 5 to 8 km except of small parts of the Walvis Basin, where up to 10 km of sediments are present. Onshore, the model also differentiates upper Proterozoic sediments (Owambo and Nama basins: (Miller, 1997; Clauer and Kröner, 1979)). The Continent-Ocean Boundary (COB; after Pawlowski (2008)) runs approximately along the 5 km isopach of the sedimentary fill and parallel to the coastline.

Below the sedimentary basins, the top-crystalline basement descends seaward. Offshore, where the Walvis Ridge intercepts the coast, the shallowest basement is at a depth of 2000 meters below sea level (BSL). With 17 km BSL the top-basement is deepest in the South-Southeast beneath the Orange Basin (Fig. 2b). The upper crystalline crustal thickness is largest onshore, with a maximum thickness of more than 45 km. Towards the COB, the thickness of the crystalline crust progressively decreases and attains less than 5 km in the oceanic crustal domain (Fig. 3a).

The depth of the Moho varies between 20 and 30 km BSL beneath the continental shelf (Fig. 3b), where the lithospheric mantle (the layer between the Moho and the Lithosphere-Asthenosphere Boundary) has the largest and smallest thickness

Solid Earth Discuss., https://doi.org/10.5194/se-2017-86
Manuscript under review for journal Solid Earth
Discussion started: 29 August 2017

beneath the onshore area, with 135 and 75 km, respectively (Fig. 3c). Beneath the sedimentary basins, the thickness of the lithospheric mantle is approximately uniform and stays in the range between 80 and 100 km.

In their 3D thermal model, Maystrenko et al. (2013), considered a temperature of 5 °C as upper thermal boundary condition at surface and seafloor, respectively. The topography and bathymetry of these surfaces is displayed in figure 4a. The topography reaches a height of more than 1500 meters above sea level (ASL) and decreases seaward. Offshore, the continental shelf is a few hundred meters BSL; the continental slope descends steeply to the isobath of 3000 meters BSL at the COB. Farther, the seafloor descends with a more gentle slope to 5000 meters BSL. In the investigated area, the deepest part of the ocean is located in the southwestern corner of the model with a depth to 5500 meters BSL.

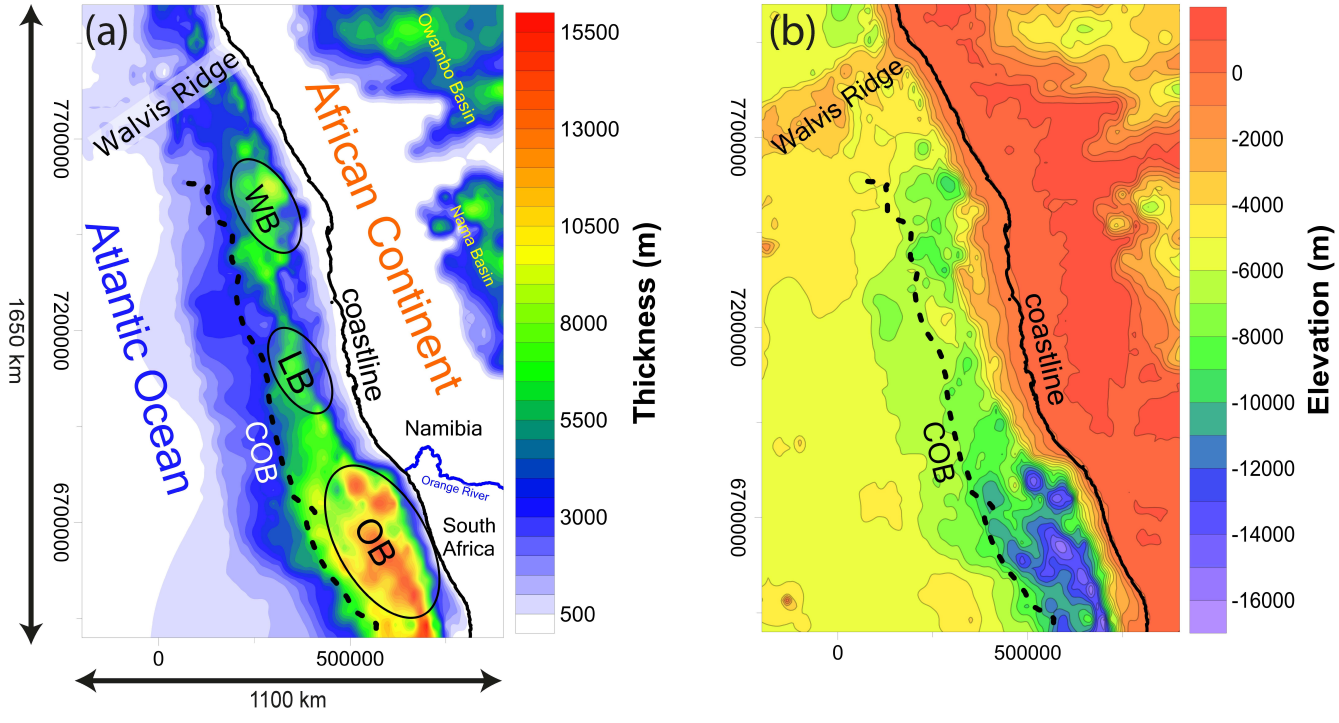

Figure 2. 3D structural model of the SW African passive margin: (a) cumulative thickness map of sediments; (b) depth to top-basement (COB: Continent-Ocean Boundary, WB: Walvis Basin, LB: Lüderitz Basin, OB: Orange Basin, UTM: WGS84, zone 33S).

Along with the top surface and the seafloor, the Lithosphere-Asthenosphere Boundary (LAB) constitutes also a crucial element in the structural/thermal model as it is the interface to which the lower thermal boundary condition of 1300 °C is assigned. The LAB is deepest (∼ -180 km) beneath the onshore areas in the Northeast and shallowest (∼ -100 km) under the oceanic region (Fig. 4b). Beneath the sedimentary basins of the continental margin, the LAB is situated at a depth of 115 to 120 km BSL, except for the southern part of the Orange Basin, where the depth of the LAB descends to 130 km BSL.

Solid Earth Discuss., https://doi.org/10.5194/se-2017-86
Manuscript under review for journal Solid Earth
Discussion started: 29 August 2017

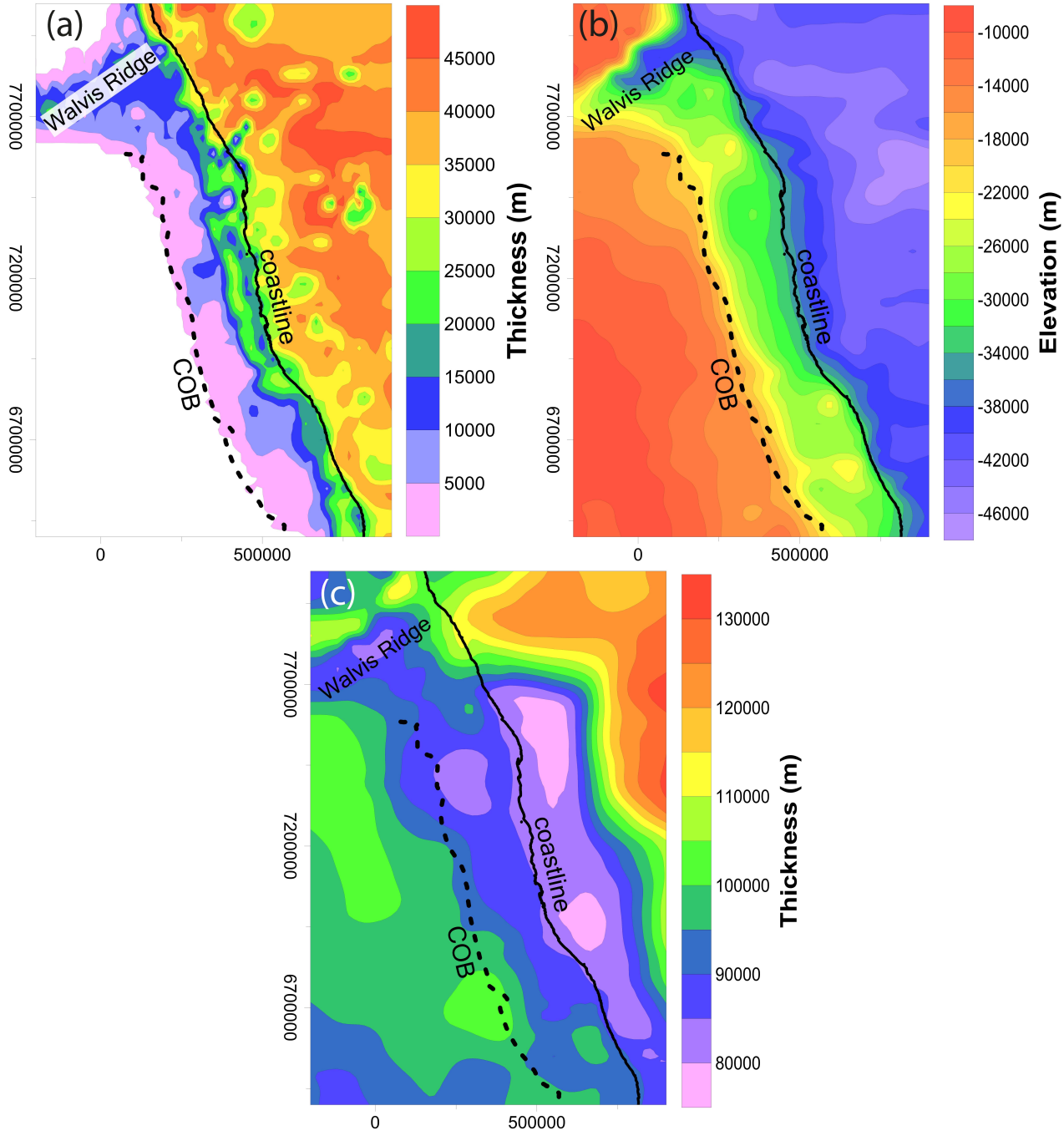

Figure 3. 3D structural model of the SW African passive margin: (a) thickness of the upper crystalline crust; (b) depth to Moho; (c) thickness of the lithospheric mantle.

Solid Earth Discuss., https://doi.org/10.5194/se-2017-86
Manuscript under review for journal Solid Earth
Discussion started: 29 August 2017

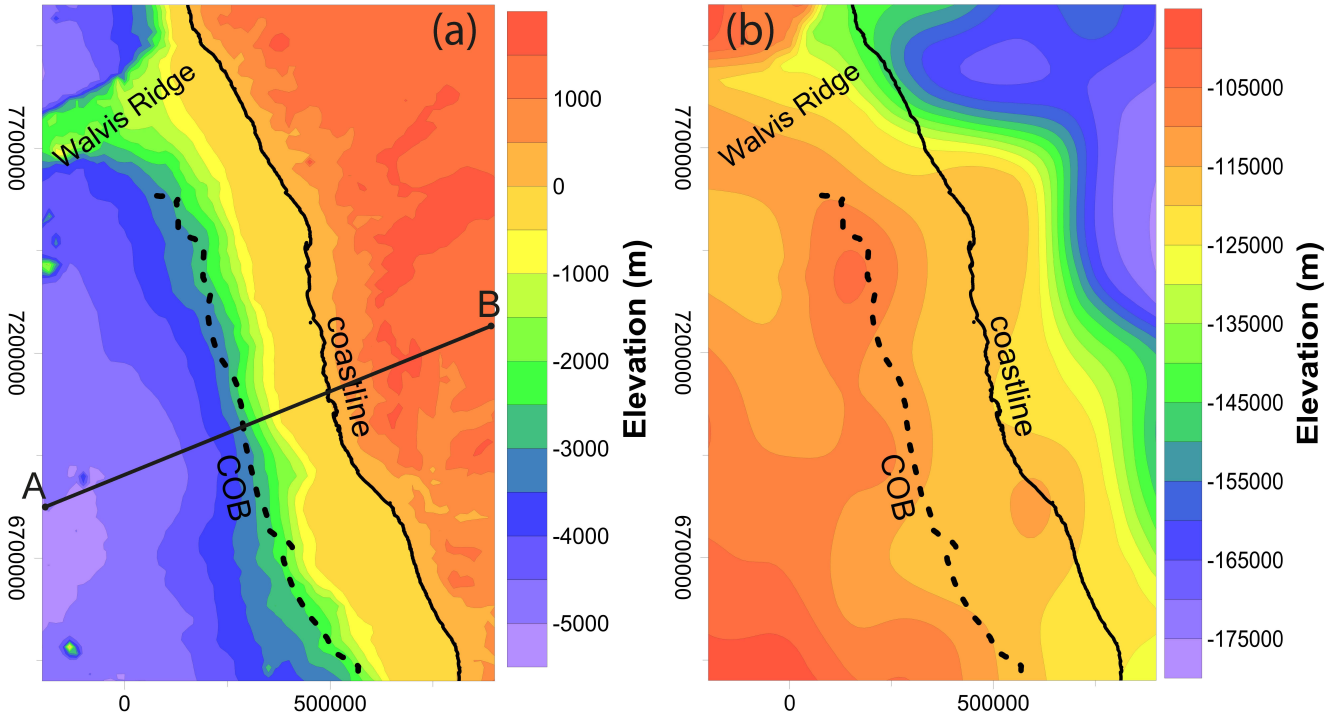

Figure 4. Surfaces with a fixed temperature for which the thermal boundary conditions were assigned to in the SW African thermal model: (a) topography–bathymetry corresponding to the upper thermal boundary condition (5 °C); (b) depth of the LAB utilized as the lower thermal boundary condition (1300 °C).

3.3 Norwegian Passive Margin

The Norwegian passive margin includes the Vøring and the Møre basins. We extracted the cumulative thickness of sediment packages from the structural model (Fig. 5a). The thickest part of the sediments lies within the Vøring Basin, with a thickness of up to 17 km. Compared to the Vøring Basin, the sediments within the Møre Basin are thinner and rarely thicker than 12 km. The sedimentary thickness is more uniform along the COB and approximately follows the 8 km isopach.

Over the whole area, the depth to the crystalline basement varies between more than 1500 meters ASL to 18 km BSL (Fig. 5b). The deepest parts of the basement are located beneath the sedimentary basins, and parallel to the COB. The depth to the top of the crystalline basement is almost uniform below the oceanic crustal domain and varies between 5 to 6 km BSL. The thickness of the upper crystalline crust (Fig. 6a) is largest onshore, with more than 35 km beneath the Norwegian Caledonides. Offshore, the thickness decreases seaward to about less than 5 km in the oceanic crustal domain.

According to the crustal structure, the Moho is deeper (17 to 37 km BSL) below the continental crust compared to the oceanic crust where the Moho is inferred to be located at a depth of 9 to 20 km BSL (Fig. 6b). Below the Moho, the thickness

Solid Earth Discuss., https://doi.org/10.5194/se-2017-86
Manuscript under review for journal Solid Earth
Discussion started: 29 August 2017

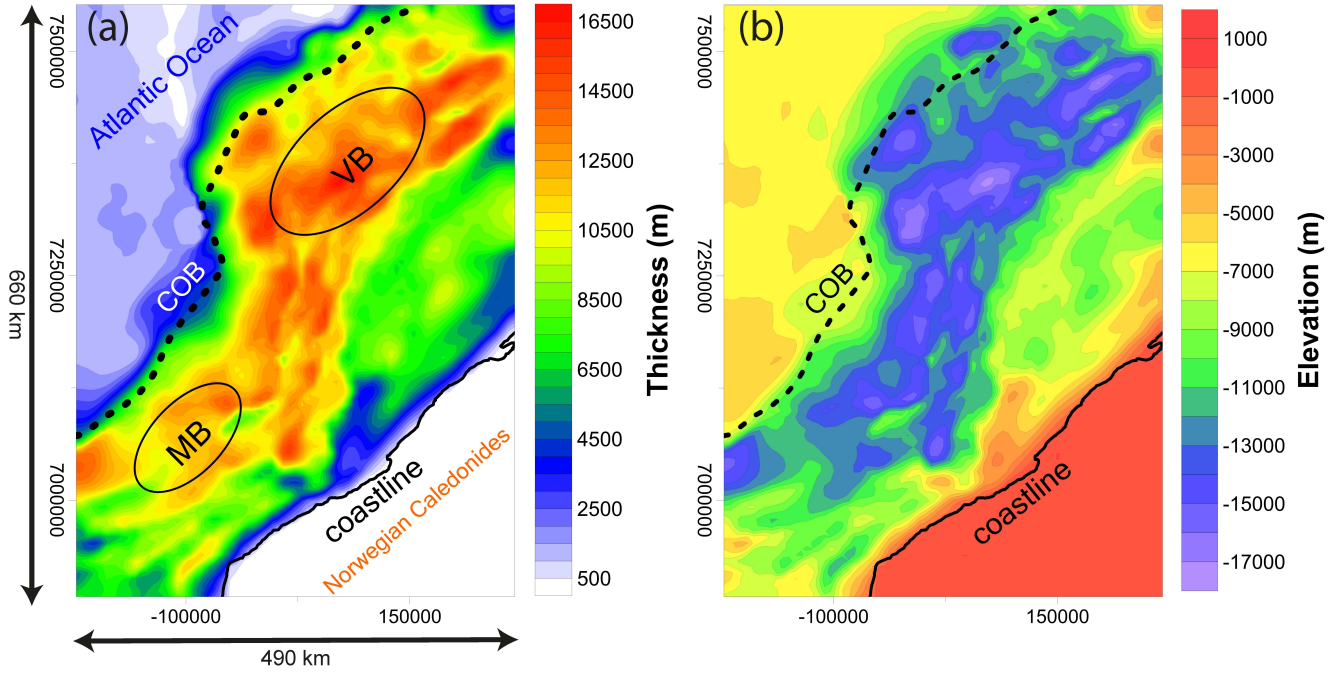

Figure 5. 3D structural model of the Norwegian margin: (a) cumulative sediment thickness; (b) depth to top-basement (COB: Continent-Ocean Boundary, VB: Vøring Basin, MB: Møre Basin, UTM: WGS84, zone 33N).

of the lithospheric mantle decreases seaward from 110 km in the continental domain to 45 km in the oceanic crustal domain (Fig. 6c).

For the thermal model (Scheck-Wenderoth and Maystrenko, 2008), a 2 °C isotherm was assigned as the upper thermal boundary condition at the topography and bathymetry (Fig. 7a). Onshore, the topography reaches elevations of close to 2000 meters ASL and descends seaward. Offshore, the wide continental shelf is a few hundred meters BSL and descends to more than 3500 meters BSL in the oceanic crustal domain.

In addition to the upper thermal boundary condition setting and equivalent to the SW African margin, the LAB surface was considered as the lower thermal boundary condition (1300 °C). The depth to the LAB (Fig. 7b) changes gradually from 55 km BSL in the oceanic crustal domain to 140 km BSL onshore.

4 Results

Our results show that the geothermal gradient varies laterally across the models' area and nonlinearly decreases with depth (Fig. 8, 9 and 10). To describe these variations, we classified these results in three different domains considering the geostructural setting; the onshore domain, the continental margin domain (the area between the coastline and the COB), and the oceanic crustal domain.

Solid Earth Discuss., https://doi.org/10.5194/se-2017-86
Manuscript under review for journal Solid Earth
Discussion started: 29 August 2017

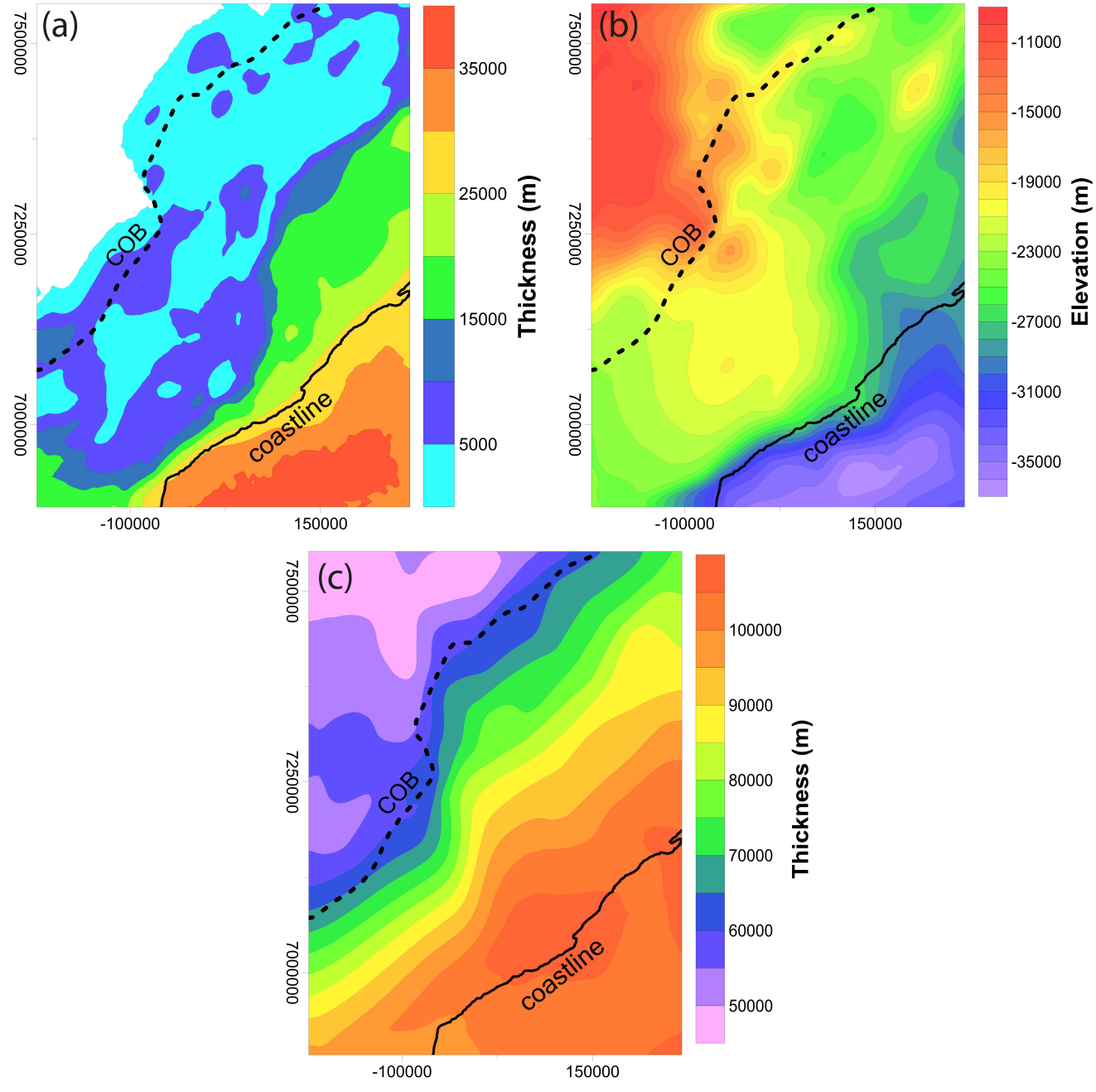

Figure 6. 3D structural model of the Norwegian margin: (a) thickness of the upper crystalline crust; (b) depth to Moho; (c) thickness of the lithospheric mantle at the Norwegian continental margin.

Solid Earth Discuss., https://doi.org/10.5194/se-2017-86
Manuscript under review for journal Solid Earth
Discussion started: 29 August 2017

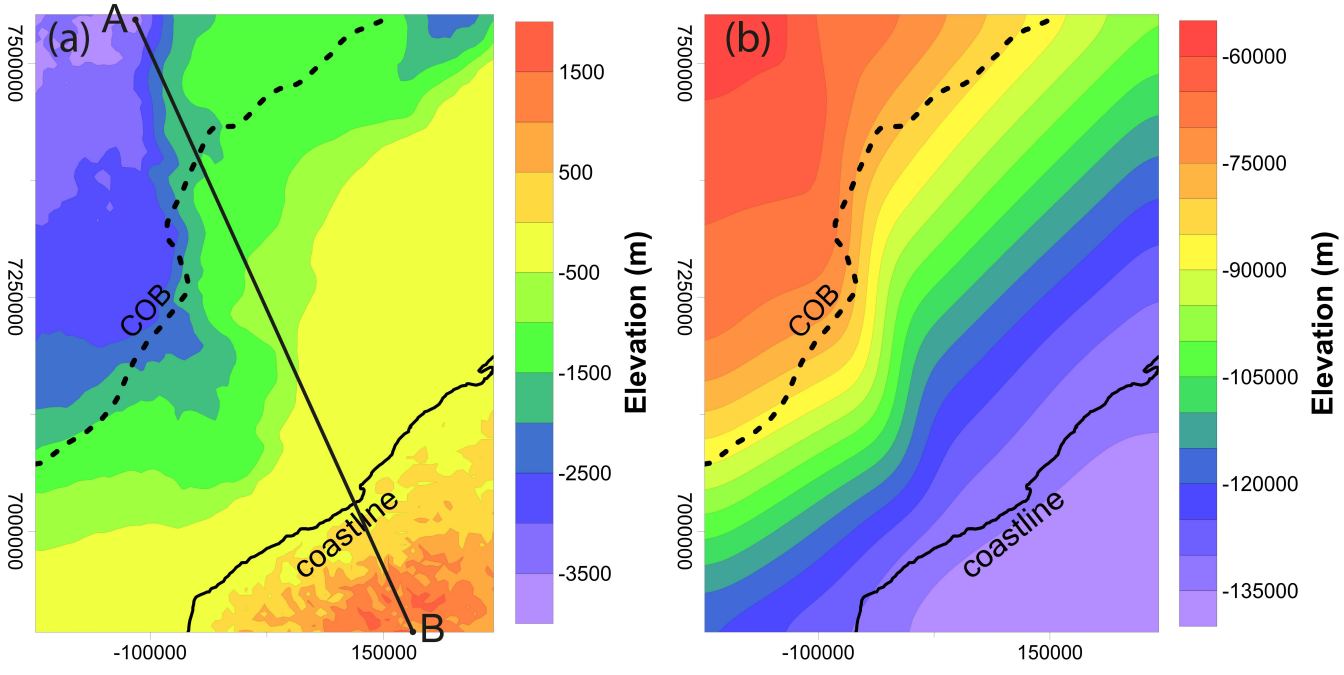

Figure 7. Surfaces with a fixed temperature for which the thermal boundary conditions were assigned to in the Norwegian thermal model: (a) topography–bathymetry corresponding to the upper thermal boundary condition (2 °C); (b) depth of the LAB utilized as the lower thermal boundary condition (1300 °C).

4.1 The Onshore Domain

In the onshore domain of the SW African model, the geothermal gradient remains in the range of 28–30 °C/km for all depth intervals except for the Precambrian basins (Fig. 8). However, there are some local depressions along the coastline. Within the 2nd (Fig. 8b) and 3rd (Fig. 8c) intervals, the geothermal gradient partly decreases to 26–28 °C/km along the coastline. Within the thicker intervals, this range covers the area more uniformly and to a greater extent (Fig. 8d, 8e, 8f).

Over the onshore domain, the geothermal gradient in the Norwegian model generally stays in the range of 15–17 °C/km for all depth intervals (Fig. 9), and this is the lowest value of the geothermal gradient across the entire model domain. Across the coastline, the geothermal gradient increases steeply seaward from 17 °C/km to 27 °C/km within the first depth interval (Fig. 9a), which is related to the transition between crystalline crust onshore and sediment fill offshore. The same pattern, but with different ranges, is also recognizable for the thicker intervals (Fig. 9).

In general, geothermal gradients in the unthinned onshore domain of the SW African margin are greater than in the corresponding domain of the Norwegian margin (Fig. 8 and 9).

Solid Earth Discuss., https://doi.org/10.5194/se-2017-86
Manuscript under review for journal Solid Earth
Discussion started: 29 August 2017

4.2 The Continental Margin Domain

In this domain, the geothermal gradient variations also reveal a general trend of reduction with increasing depth. Nevertheless, this general trend displays different lateral variations for each sedimentary basin.

4.2.1 The SW African Passive Margin

In the SW African model, the results display different patterns of variation for the individual depth intervals. Within the first depth interval (Fig. 8a), the variations are similar in the Walvis and Lüderitz basins. The geothermal gradient increases seaward from the coast and reaches the largest value (48–50 °C/km) in the central parts of the sedimentary basins where the sediments are thickest (Fig. 2a). Oceanward, the gradient declines again towards the distal shelf where the geothermal gradient is in the range of 38–40 °C/km along the COB. In contrast, the geothermal gradient follows a different pattern within the Orange Basin. It decreases with distance from the coast, reaches the lowest value (34–36 °C/km) in the central part of the basin and then increases to the COB. The reduced gradient within the first depth interval in the Orange Basin compared to the two other basins corrolates with an increased thickness of the uppermost sedimentary unit of the Cenozoic. This unit has the lowest thermal conductivity of the sedimentary units (Table 1) and is almost absent in the central part of the Orange Basin (Maystrenko et al., 2013).

The variations of the geothermal gradient within the second, the third, and the fourth depth intervals (Fig. 8b, 8c & 8d) follow the same trend as in the first depth interval. A notable difference between these three depth intervals (2nd, 3rd, and 4th) and the first depth interval is the location of the highest geothermal gradient. Within the second, third, and fourth depth intervals, theses high values occur in the northern part of the Walvis Basin; this contrasts with the first depth interval where the highest value was found in the Lüderitz Basin (Fig. 8a). These high values are in the ranges of 44–46 °C/km, 42–44 °C/km and 40–42 °C/km within the second, the third, and the fourth depth intervals, respectively. This difference is explicable by considering the top-basement depth (Fig. 2b) and the crustal thickness (Fig. 3a), which are shallower and thicker beneath the northern part of the Walvis Basin compared to the Lüderitz Basin. Moreover, the youngest sediments (with lower thermal conductivity) are thickest in the Walvis Basin (Table 1, Maystrenko et al. (2013)), which is an additional reason for these values of high geothermal gradient within the Walvis Basin.

Within the two thickest depth intervals (5 and 6 km), the results show a different pattern of the geothermal gradient variations within the Orange Basin (Fig. 8e & 8f). Unlike the upper depth intervals the geothermal gradient varies in a similar manner to the Walvis and Lüderitz basins. The geothermal gradient increases seaward from the coast, reaches the locally highest value in the central part of the sedimentary basin, and finally declines towards the COB.

Overall, in the SW African model, the highest values of the geothermal gradient for all depth intervals occur within the sedimentary basins (Fig. 8).

Solid Earth Discuss., https://doi.org/10.5194/se-2017-86
Manuscript under review for journal Solid Earth
Discussion started: 29 August 2017

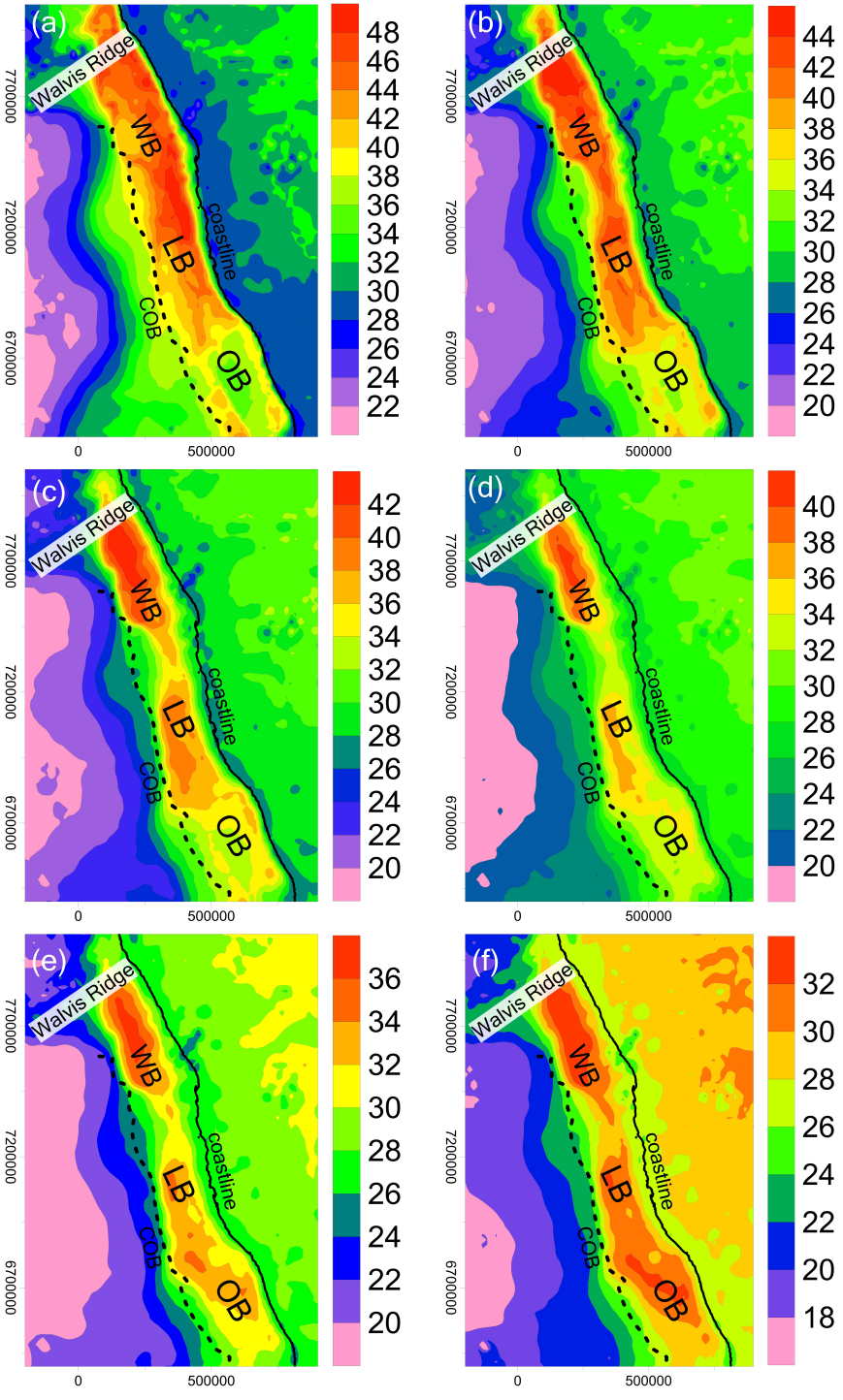

Figure 8. Geothermal gradients [°C/km] at the SW African passive margin for (a) 1, (b) 2, (c) 3, (d) 4, (e) 5, and (f) 6 km below the topography–bathymetry (which was assigned a constant temprature of 5 °C).

Solid Earth Discuss., https://doi.org/10.5194/se-2017-86
Manuscript under review for journal Solid Earth
Discussion started: 29 August 2017

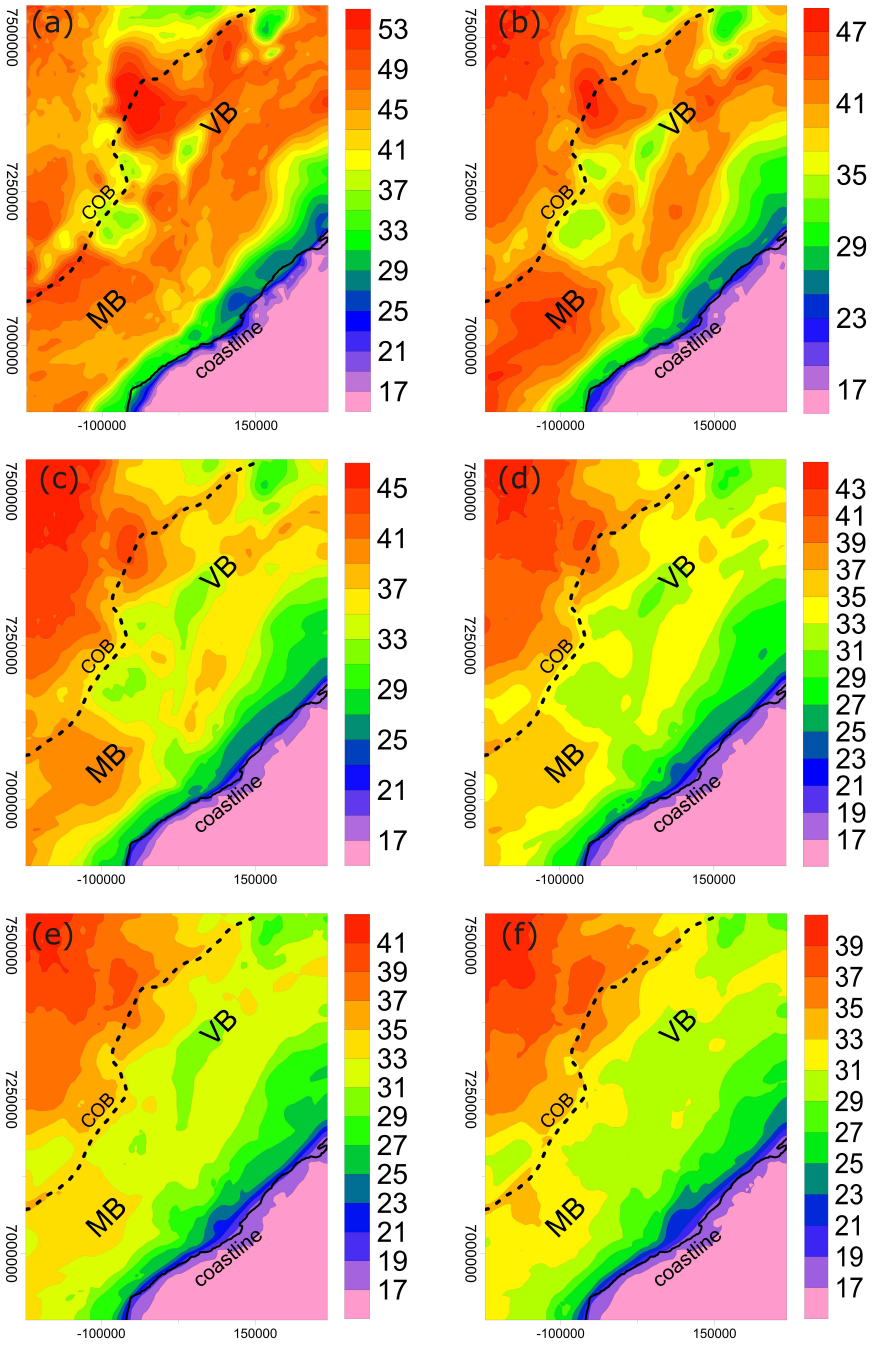

Figure 9. Geothermal gradients [°C/km] at the Norwegian passive margin for (a) 1, (b) 2, (c) 3, (d) 4, (e) 5, and (f) 6 km below the the topography–bathymetry (which was assigned a constant temprature of 2 °C).

Solid Earth Discuss., https://doi.org/10.5194/se-2017-86
Manuscript under review for journal Solid Earth
Discussion started: 29 August 2017

4.2.2 The Norwegian Margin

The geothermal gradient distribution maps of the Norwegian margin (Fig. 9) also reveal lateral and vertical variations across the sedimentary basins.

In the Vøring Basin, the geothermal gradient varies in a similar manner for all depth intervals, except the thickest interval (Fig. 9). Generally, the gradient increases seaward from the coast, decreases in the central part of the basin, and then increases again toward the COB. Similar to the Orange Basin at the SW African margin, the decrease of the gradient is akin to the central part of the Vøring Basin, where the uppermost Cenozoic sedimentary unit with the lowest thermal conductivity (Table 1) is absent (Scheck-Wenderoth et al., 2007). Within the thickest depth interval (Fig. 9f), the geothermal gradient increases gradually from the coast towards the COB and no reduction occurs in the central part of the basin. The highest values of the geothermal gradient, within the Vøring Basin, are found at the distal shelf. These values are in the range of 53–55 °C/km in the first depth interval and attain 35–37 °C/km within the thickest depth interval.

In contrast to the Vøring Basin, the geothermal gradient within the Møre Basin does not follow a comparable pattern in the first two depth intervals. Within the first interval, the geothermal gradient increases gradually and continuously from the coast towards the COB (Fig. 9a). In the second depth interval, the geothermal gradient increases from the coast to the central part of the basin and decreases towards the COB (Fig. 9b). Within the other four thicker depth intervals (Fig. 9c to 9f), the general trend of the geothermal gradient variations is similar to the first depth interval.

4.3 The Oceanic Crustal Domain

The oceanic crustal domain refers to the western side of the COB where the crust is mainly oceanic in composition. Herein, the geothermal gradient variations differ significantly between the SW African and the Norwegian margins.

In the SW African model, the results of the calculated geothermal gradient (Fig. 8) for the oceanic crustal domain and within all the depth intervals indicate a lateral oceanward decrease. The geothermal gradient gradually decreases oceanward from the COB to reach the minimum at the western model boundary. These lowest values are in the range of 16–18 °C/km within the thickest depth interval, and 18–20 °C/km within the other five intervals and representing the lowest value of the geothermal gradient over the entire model of the SW African Margin (Fig. 8 and 11c).

In contrast, the results for the Norwegian setting (Fig. 9) show that the geothermal gradient increases oceanward in the oceanic crustal domain, where the highest values of the geothermal gradients over the entire margin are found (Fig. 9 and 11c). From the first depth interval down to the thickest depth interval, these high values stepwise decrease from 53–55, 47–49, 45–47, 43–45, 41–43, to 39–41 °C/km. The age of the oceanic crust (Table 1) and the related age-controlled depth of the thermal LAB (Fig. 4a and 7a) would be a reasonable explanation for this difference within the oceanic crustal domain of the two differently aged margins. At the older SW African passive margin the shallowest depth to the LAB is around 100 BSL km below the oceanic crustal domain (Fig. 4b), while the LAB depth at the younger Norwegian margin is less than 60 km BSL (Fig. 7b).

Solid Earth Discuss., https://doi.org/10.5194/se-2017-86
Manuscript under review for journal Solid Earth
Discussion started: 29 August 2017

5 Interpretation and Discussion

According to our results, the calculated geothermal gradients reveal variations both laterally and with depth for the two different passive margin (Fig. 8 and 9). In general, the geothermal gradient decreases nonlinearly with depth in both models. However, this occurs in different trends for the two settings. Calculation of the geometric mean value of the geothermal gradient fully shows nonlinear decreasing from the first depth interval to the thickest depth interval by 40 °C/km to 30 °/km in the Norwegian margin and by more than 32 °C/km to less than 26 °C/km in the SW African margin (Fig. 10). To address the differences between the present-day thermal field of the SW African passive margin and the Norwegian margin, it is important to compare the geothermal gradient variations with the geological structure, the thermal properties of comparing geological units, and the ages of the oceanic crust (Table 1). A structural-thermal cross section (Fig. 11a and b) and corresponding profile of average geothermal gradient (Fig. 11c) provide supplemental indications for a valid interpretation of shallow thermal filed variations across the two differently aged passive margins. We will discuss these issues with regards to the three previously mentioned domains: (1) the onshore domain, (2) the continental margin domain, and (3) the oceanic crustal domain.

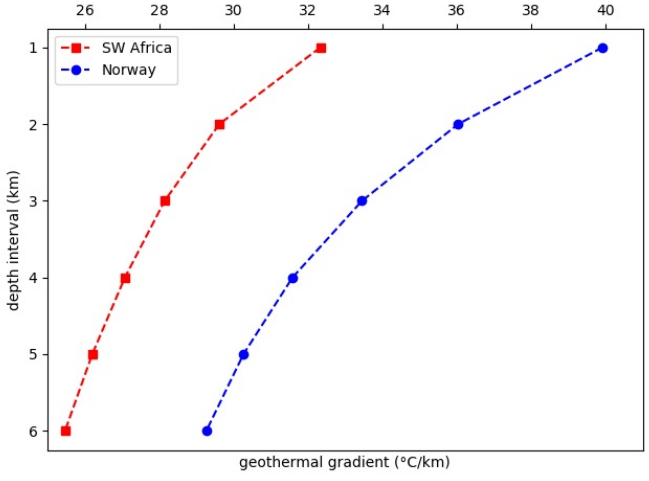

Figure 10. Mean values of the geothermal gradient [°C/km] for the different depth intervals.

Temprature-depth function is simply a linear concept of the geothermal gradient (Eq. 3). However, as can be seen from the two models, the geothermal gradient depends on the considered depth interval and varies nonlinearly with depth. The solution to the steady-state thermal diffusion equation (Eq. 4 derived from Eq. 2) is a second-order (nonlinear) temperature function of depth if radiogenic heat production is considered ($S \neq 0$). This fact indicates that the temperature-depth ($T - z$) curvature is highly sensitive to the amount of radiogenic heat production. The interaction of the thermal conductivity of different lithospheric layers and the heat internally produced by the decay of radioactive elements overprint the heat input from larger

Solid Earth Discuss., https://doi.org/10.5194/se-2017-86
Manuscript under review for journal Solid Earth
Discussion started: 29 August 2017

mantle depth into the lithosphere (Eq. 4). For better comprehension and further comparability, investigating the variability of the geothermal gradient requires representing the same depth intervals across the study areas.

$$\frac{\partial^2 T}{\partial z^2} = \frac{S}{\lambda} \tag{4}$$

5.1 The Onshore Domain

In the onshore domain, the geothermal gradient is considerably higher ($\sim$ 13 °C/km) at the SW African margin compared to the Norwegian margin. The SW African margin has a thicker crust compared to the Norwegian margin (Fig. 3a, 6a, 11a) and thus relatively more radiogenic heat is contributed by the crust. Additionally, a second reason could be the assigned values of radiogenic heat production in the thermal models (see Eq. 4). In the Norwegian model, Scheck-Wenderoth and Maystrenko (2008), considered an average crustal radiogenic heat production as 0.8 [$\mu W/m^3$] which is much lower than the corresponding value (1.45 [$\mu W/m^3$]) in the SW African thermal model (Table 1). This low value of the geothermal gradient within the onshore domain in the Norwegian model agrees with downhole temperature measurements in the Scandinavian Caledonides that imply an average geothermal gradient of $\sim$ 17–20 °C/km (e.g., Maystrenko et al., 2015; Lorenz et al., 2015; Pascal, 2015).

Another impressive characteristic of the thermal field of these two passive margins exists in the vicinity of the coastline. Here, the geothermal gradient decreases by about 2 °C/km at the SW African margin. This reduction spatially correlates with the crustal thickness decrease ($\sim$ 10 km) beneath the coast (Fig. 2b). The thinner crust produces less radiogenic heat, which leads to lower temperatures. In contrast, considering the same area at the Norwegian margin, the geothermal gradient increases by approximately 10 °C/km within the first depth interval and gradually decreases within the deeper depth intervals. These variations might be explained by the thermal blanketing effect of the up to 1.5 km thick insulating sediments (low thermal conductivity, Table 1) along the coast (Fig. 5a). While the outcropping crystalline crust onshore efficiently transports heat to the surface in response to its greater thermal conductivity, the heat is stored in the insulating sediments offshore.

5.2 The Continental Margin Domain

To interpret the thermal field variations within the sedimentary basins, and to compare these differences between the SW African and the Norwegian margins, we need to take a closer look at the geometry of the geological structural units within and beneath the location of the sedimentary basins. These units were presented in section 3 and here we will discuss how they affect the thermal field.

5.2.1 The SW African Passive Margin

Considering the geothermal gradient variations over the whole study area at the SW African passive margin, the highest values for the geothermal gradient occur within the sedimentary basin areas. Beneath the continental margin, the crystalline crust is thinner (i.e. less radiogenic heat production) in comparison to the onshore domain (Fig. 2b). Moreover, the LAB is also deeper beneath the sedimentary basins compared to the LAB depth below the oceanic crustal domain (Fig. 4b). Accordingly, in spite

Solid Earth Discuss., https://doi.org/10.5194/se-2017-86
Manuscript under review for journal Solid Earth
Discussion started: 29 August 2017

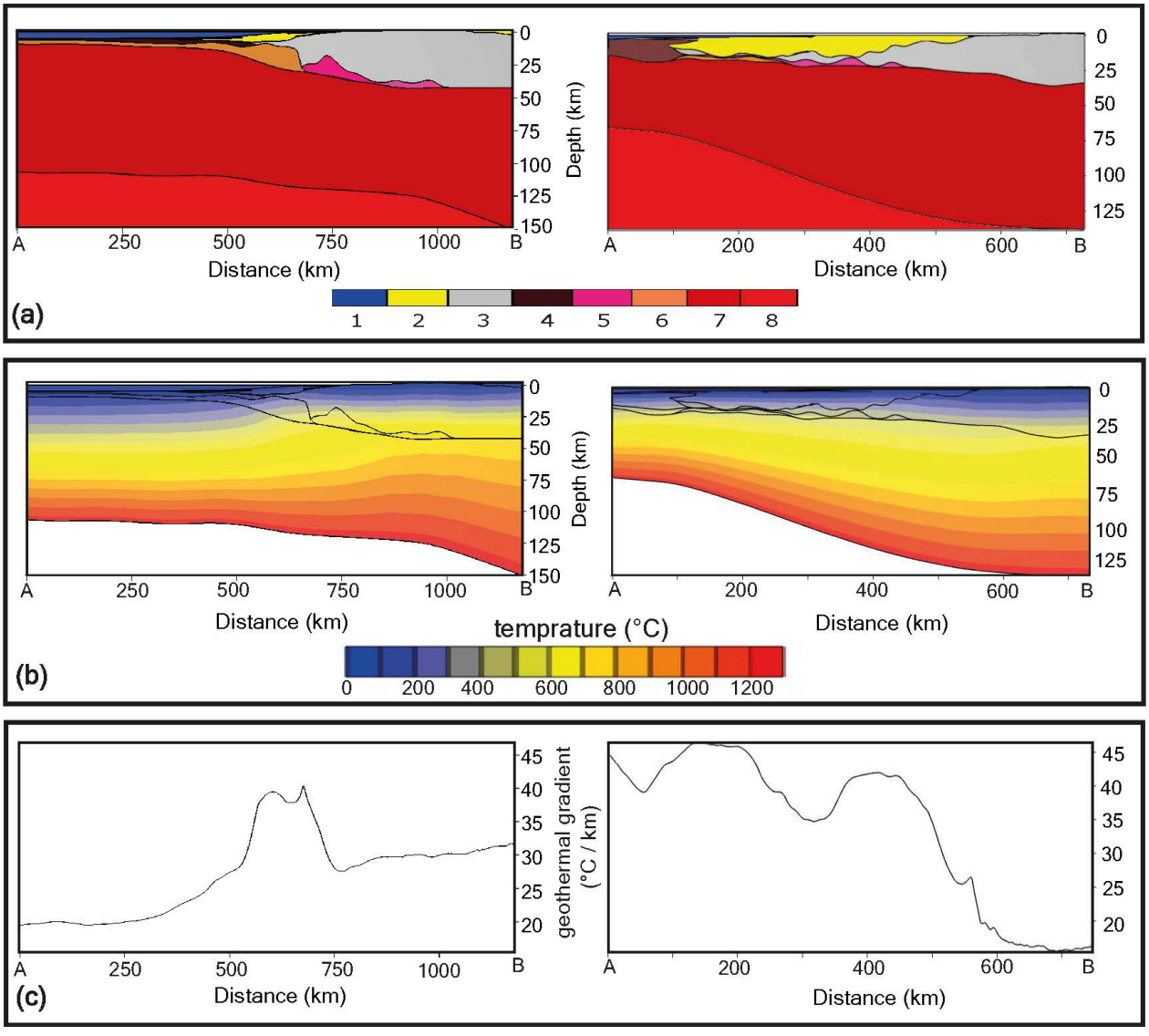

Figure 11. Structural-thermal cross section and corresponding average geothermal gradient at SW African passive margin (left) and Norwegian continental margin (right) after Maystrenko et al. (2013); Scheck-Wenderoth et al. (2007); Scheck-Wenderoth and Maystrenko (2008): (a) Structural crustal cross section along A–B profile (Fig. 4a and Fig. 7a). Numbers near color legend for individual layers: 1) water, 2) sediments, 3) crystalline continental crust, 4) oceanic crust, 5) high-density continental crust, 6) high-velocity high-density lower crustal layer, 7) low density mantle, 8) normal density mantle. (b) Temperature distrbution within the A–B cross section. (c) Calculated average geothermal gradient along the A–B cross section.

Solid Earth Discuss., https://doi.org/10.5194/se-2017-86
Manuscript under review for journal Solid Earth
Discussion started: 29 August 2017

of a lower radiogenic heat production and a larger depth to the thermal LAB, the gradients are highest in the sedimentary part. This indicates that the thermal blanketing effect of the insulating sediments has the strongest control on the shallow thermal field variations within the sedimentary basins, and geothermal gradients widely correlate positively with sediment thickness.

The top-basement (Fig. 2b) is much deeper below the Orange Basin and the radiogenic crust thinner compared to the Walvis and Lüderitz basins ($\sim$ 10 km difference in the center of the sedimentary basins). Accordingly, the thicker sediments within the Orange Basin (Fig. 2a) lead to a more pronounced thermal blanketing effect due to the low thermal conductivity of these sediments. Additionally, Cenozoic sediments with lower thermal conductivity are thicker in the Walvis and Lüderitz basins compared with the Orange Basin (Table 1, Maystrenko et al. (2013)). These differences in the top-basement depth and the thickness of younger sediments with low thermal conductivity would explain why the geothermal gradient has the lowest local value in the central part of the Orange Basin in the upper depth intervals, 1 to 4 km below the upper thermal boundary condition. Within the thicker depth intervals, between 4 and 6 km below the upper thermal boundary condition, all sediments have a Cretaceous age (Table 1, Maystrenko et al. (2013)). Consequently, the thermal field pattern shows more similarity within all the three sedimentary basins and the geothermal gradient increases toward their central part (Fig. 8e & 8f).

5.2.2 The Norwegian Margin

In general, the geothermal gradient variations within the sedimentary basins show fewer complexities at the Norwegian margin in comparison to the SW African passive margin. Within the Vøring Basin and for all depth intervals, the geothermal gradient generally increases seaward, decreases in the central part of the basins, but increases again toward the distal shelf (Fig. 9). While the crystalline crust is thinner (i.e. less radiogenic heat is produced) beneath the sedimentary basins compared to the onshore domain (Fig. 6a), the lithospheric mantle (Fig. 6c) gradually thins and the LAB (Fig. 7b) becomes progressively shallower towards the ocean. In addition, the lack of the post-breakup (uppermost Cenozoic) sedimentary unit in the central part of the Vøring Basin reduces the thermal blanketing effect of insulating sediments (Table 1, Scheck-Wenderoth et al. (2007)). With increasing depth, the thermal blanketing effect of Cenozoic sediments gets less relevant for the thermal field variations, while the depth to the LAB plays a more prominent role. As shown in Fig. 9f the geothermal gradient reveals no depression in the central part of the Vøring Basin, but increases seaward due to the shallower LAB and the thinner lithospheric mantle. The same reason would explain the geothermal gradient pattern that characterizes the More Basin. Overall, the pattern of the shallow thermal field looks similar for all depth intervals in the More Basin, increasing gradually from the continental shelf towards the distal shelf. This trend agrees with the oceanward shallowing LAB depth.

The absolute values of the geothermal gradient within the sedimentary basins in the Norwegian model are larger compared to the corresponding values in the SW African model. The highest geothermal gradient at the SW African passive margin occurs within the sedimentary basins (Sec. 5.2.1), whereas this is not the case for the Norwegian model. In addition to the quantitative differences, these high values exist within the central part of the sedimentary basins at the SW African margin, while for the Norwegian model the highest local values of the geothermal gradient in the continental margin domain occur closer to the distal shelf. These differences indicate fundamentally different controlling factors for the shallow thermal field at these two differently aged passive margins.

Solid Earth Discuss., https://doi.org/10.5194/se-2017-86
Manuscript under review for journal Solid Earth
Discussion started: 29 August 2017

5.3 The Oceanic Crustal Domain

The oceanic crustal domain is most important for comparing the shallow thermal field variations for the SW African passive margin and the Norwegian margin. While the SW African model has the lowest values of the geothermal gradient in this domain (Fig. 8), the Norwegian model presents the highest value of the geothermal gradient (Fig. 9).

The volcanic passive margin of Norway (55 Ma) is significantly younger than the SW African passive margin (130 Ma). This age contrast resulted in around 40 km depth difference of the thermal LAB for these two passive margins (Fig. 4b & Fig. 7b). The consequence of this shallower oceanic LAB is a steeper average geothermal gradient as the 1300 °C difference between surface and LAB needs to be accommodated within 60 km. This distance is almost twice as large at the SW African margin where the oceanic LAB is at 110 km depth. Accordingly, the young Norwegian margin is hotter in comparison to the old SW African margin, which appears to be thermally equilibrated (Maystrenko et al., 2013).

With respect to the hypothesis formulated in the introduction, our research suggests that knowing or considering variations in the crust alone is not sufficient to properly assess present or the past configuration of the geothermal gradient of passive continental margin.

5.4 Implications

Methods of thermal history reconstruction are mostly based on paleotemperature indicators, that experience irreversible structural changes when passing through a certain temperature window (Allen and Allen, 2005; Naeser and McCulloh, 2012). The thermal alteration of organic matter for example results in specific changes of vitrinite reflectivity and linear relationships between temperature and vitrinite reflectivity have been established using lab experiments (Burnham and Sweeney, 1989; Dow, 1977; Corcoran and Clayton, 2001; Barker and Pawlewicz, 1986). Likewise, Apatite Fission Track Analysis makes use of the specific temperature-dependent behaviour of fission track in response to radiogenic decay (Barker, 1996; Gallagher et al., 1998; Stockli et al., 2000; Reiners and Brandon, 2006; Deeken et al., 2006). Such paleotemperature indicators are often translated to amounts of paleo-burial depth assuming a constant paleo-thermal gradient for a certain study area and the difference between the present-day depth and the paleo-depth is interpreted in terms of vertical movements. Our results indicate that the thermal gradient may vary significantly both laterally and with time (Fig. 11). Accordingly assuming an average paleo-thermal gradient of 30 °C/km positions the 70°C window of an Apatite sample at 2 to 3 km depth whereas a higher paleo-geothermal gradient of 45 °C/km would position the same sample at 1.5 km depth. Therefore, considering paleo-geothermal gradient variation in response to sedimentation or lithosphere cooling is key if paleo-temperatures, paleo-elevations and, derived from the latter, vertical movements are deduced. This implies that in addition to the general paleotectonic setting, also the evolutionary phase and the position in this setting need to be considered. For passive margin settings this means that it is not only important to take into account the type of passive margin (magma-rich versus magma-poor) but also the location (relative to the continent and to the newly formed oceanic domain) and the time with respect to break up are relevant to consider. A sample from a proximal or distal domain at an early or late stage of evolution has experienced different thermal imprints and the paleo-position should be considered accordingly in thermal history reconstruction.

Solid Earth Discuss., https://doi.org/10.5194/se-2017-86
Manuscript under review for journal Solid Earth
Discussion started: 29 August 2017

6 Conclusions

The assessment of variations in the geothermal gradient for the two different passive volcanic margins revealed that:

- In spite of a similar crustal structure, the geothermal gradient differs laterally across the two passive margins and non-linearly decreases with depth.
- The thermal field of the two margins is contrasting. At the Norwegian margin (young) the thermal field is mostly dominated by the thermo-tectonic age and the thermal LAB depth in contrast to the SW African margin (old) where the crustal configuration is dominating the pattern of the equilibrated shallow thermal field.
- Over the onshore domain, the radiogenic heat production is the main heat controlling factor for both settings. Within the sedimentary basins, the thermal blanketing effect of the insulating sediments has the highest impact on the shallow thermal field at both margins. In the oceanic crustal domain, the thermal field is highly affected by the age of the ocean and the thermal LAB depth. Therefore, the Norwegian model is significantly hotter than the SW African model in the oceanic crustal domain and of the distal margin.
- While the causative thermal anomaly leading to margin formation in the South Atlantic should be equilibrated, the thermal disturbance in the North Atlantic and the proximity to the Iceland plume obviously cause thermal effects at present-day. Characteristics of the lithosphere ultimately determine the thermal field for the two settings.
- This fact that the geothermal gradient is nonlinear and varies across areas has implications for methods of thermal history reconstruction.

Competing interests. The authors declare that they have no conflict of interest.

Acknowledgements. The research leading to these results has received funding from the People Programme (Marie Curie Actions) of the European Union's Seventh Framework Programme FP7/2007-2013/ under REA grant agreement n° [607996]. We are very grateful to Yuriy P. Maystrenko for his feedback on the database, and to Jessica Freymark for her methodological support. All data for this paper is properly cited and referred to in the reference list.

Solid Earth Discuss., https://doi.org/10.5194/se-2017-86
Manuscript under review for journal Solid Earth
Discussion started: 29 August 2017

References

Allen, P. A., and Allen, J. R. (2005). Basin analysis: Principles and application to petroleum play assessment. Blackwell, Oxford.

Artemieva, I. M. (2006). Global 1× 1 thermal model TC1 for the continental lithosphere: implications for lithosphere secular evolution. Tectonophysics, 416(1), 245–277.

Artemieva, I. M., and Mooney, W. D. (2001). Thermal thickness and evolution of Precambrian lithosphere: a global study. Journal of Geophysical Research: Solid Earth, 106(B8), 16387–16414.

Balling, N., Poulsen, S. E., Fuchs, S., Mathiesen, A., Bording, T. S., Nielsen, S. B., and Nielsen, L. H. (2016). Development of a numerical 3D geothermal model for Denmark. In European Geothermal Congress 2016.

Barker, C. (1996). Thermal modeling of petroleum generation: theory and applications. Developments in petroleum science.

Barker, C. E., and Pawlewicz, M. J. (1986). The correlation of vitrinite reflectance with maximum temperature in humic organic matter. In Paleogeothermics (pp. 79–93). Springer Berlin Heidelberg.

Blaich, O. A., Faleide, J. I., Tsikalas, F., Franke, D., and León, E. (2009). Crustal-scale architecture and segmentation of the Argentine margin and its conjugate off South Africa. Geophysical Journal International, 178(1), 85–105.

Blystad, P., Brekke, H., Faerseth, R.B., Larsen, R.B., Skogseid, J., and Torudbakken, B. (1995). Structural Elements of the Norwegian Continental Shelf. Pt. 2: The Norweigan Sea Region. Norwegian Petroleum Directorate Bulletin, 8.

Brekke, H. (2000). The tectonic evolution of the Norwegian Sea continental margin, with emphasis on the Voring and More basins. Special Publication-Geological Society of London, 167, 327–378.

Brown, L. F., Benson, J. M., Brink, G. J., Doherty, S., Jollands, A., Jungslager, E. H. A., and Van Wyk, N. J. S. (1995). Sequence Stratigraphy on Offshore South African Divergent Basins. American association of petroleum geologists.

Burnham, A. K., and Sweeney, J. J. (1989). A chemical kinetic model of vitrinite maturation and reflectance. Geochimica et Cosmochimica Acta, 53(10), 2649-2657.

Chapman, D. S. (1986). Thermal gradients in the continental crust. Geological Society, London, Special Publications, 24(1), 63–70.

Clauer, N., and Kröner, A. (1979). Strontium and argon isotopic homogenization of pelitic sediments during low-grade regional metamorphism: the Pan-African upper Damara sequence of northern Namibia (South West Africa). Earth and planetary science letters, 43(1), 117–131.

Corcoran, D. V., and Clayton, G. (2001). Interpretation of vitrinite reflectance profiles in sedimentary basins, onshore and offshore Ireland. Geological Society, London, Special Publications, 188(1), 61–90.

Davies, G. F. (1980). Thermal histories of convective Earth models and constraints on radiogenic heat production in the Earth. Journal of Geophysical Research: Solid Earth, 85(B5), 2517–2530.

Deeken, A., Sobel, E. R., Coutand, I., Haschke, M., Riller, U., and Strecker, M. R. (2006). Development of the southern Eastern Cordillera, NW Argentina, constrained by apatite fission track thermochronology: From early Cretaceous extension to middle Miocene shortening. Tectonics, 25(6).

Doré, A. G., Lundin, E. R., Jensen, L. N., Birkeland, Ø., Eliassen, P. E., and Fichler, C. (1999). Principal tectonic events in the evolution of the northwest European Atlantic margin. In Geological society, london, petroleum geology conference series, vol. 5, No. 1, pp. 41–61, Geological Society of London.

Doré, A. G., Cartwright, J. A., Stoker, M. S., Turner, J. P., and White, N. J. (2002). Exhumation of the North Atlantic margin: introduction and background. Geological Society, London, Special Publications, 196(1), 1–12.

Dow, W. G. (1977). Kerogen studies and geological interpretations. Journal of geochemical exploration, 7, 79–99.

Ebbing, J., Gernigon, L., Pascal, C., Olesen, O., and Osmundsen, P. T. (2009). A discussion of structural and thermal control of magnetic anomalies on the mid-Norwegian margin. Geophysical Prospecting, 57(4), 665–681.

Franke, D. (2013). Rifting, lithosphere breakup and volcanism: Comparison of magma-poor and volcanic rifted margins. Marine and Petroleum geology, 43, 63–87.

Gallagher, K., Brown, R., and Johnson, C. (1998). Fission track analysis and its applications to geological problems. Annual Review of Earth and Planetary Sciences, 26(1), 519–572.

Gernigon, L., Ringenbach, J. C., Planke, S., and Le Gall, B. (2004). Deep structures and breakup along volcanic rifted margins: insights from integrated studies along the outer Vøring basin (Norway). Marine and Petroleum Geology, 21(3), 363–372.

Gernigon, L., Lucazeau, F., Brigaud, F., Ringenbach, J. C., Planke, S., and Le Gall, B. (2006). A moderate melting model for the Vøring margin (Norway) based on structural observations and a thermo-kinematical modelling: Implication for the meaning of the lower crustal bodies. Tectonophysics, 412(3), 255–278.

Grevemeyer, I., and Villinger, H. (2001). Gas hydrate stability and the assessment of heat flow through continental margins. Geophysical Journal International, 145(3), 647–660.

Hinz, K. (1981). A hypothesis on terrestrial catastrophes.

Larson, R. L., and Ladd, J. W. (1973). Evidence for the opening of the South Atlantic in the Early Cretaceous.

Lorenz, H., Rosberg, J. E., Juhlin, C., Bjelm, L., Almqvist, B. S. G., Berthet, T., ... and Pedersen, K. (2015). COSC-1-drilling of a subduction-related allochthon in the Palaeozoic Caledonide orogen of Scandinavia. Scientific Drilling, 19, 1.

Macdonald, D., Gomez-Perez, I., Franzese, J., Spalletti, L., Lawver, L., Gahagan, L., ... and Paton, D. (2003). Mesozoic break-up of SW Gondwana: implications for regional hydrocarbon potential of the southern South Atlantic. Marine and Petroleum Geology, 20(3), 287–308.

Maystrenko, Y. P., Scheck-Wenderoth, M., Hartwig, A., Anka, Z., Watts, A. B., Hirsch, K. K., and Fishwick, S. (2013). Structural features of the Southwest African continental margin according to results of lithosphere-scale 3D gravity and thermal modelling. Tectonophysics, 604, 104–121.

Maystrenko, Y. P., Slagstad, T., Elvebakk, H. K., Olesen, O., Ganerød, G. V., and Rønning, J. S. (2015). New heat flow data from three boreholes near Bergen, Stavanger and Moss, southern Norway. Geothermics, 56, 79–92.

McKenzie, D., Jackson, J., and Priestley, K. (2005). Thermal structure of oceanic and continental lithosphere. Earth and Planetary Science Letters, 233(3), 337–349.

Miller, R. M. (1997). The Owambo basin of northern Namibia. Sedimentary Basins of the World, 3, 237–268.

Müller, R. D., Sdrolias, M., Gaina, C., and Roest, W. R. (2008). Age, spreading rates, and spreading asymmetry of the world's ocean crust. Geochemistry, Geophysics, Geosystems, 9(4).

Muffler, P., and Cataldi, R. (1978). Methods for regional assessment of geothermal resources. Geothermics, 7(2-4), 53–89.

Mutter, J. C., Talwani, M., and Stoffa, P. L. (1982). Origin of seaward-dipping reflectors in oceanic crust off the Norwegian margin by "subaerial sea-floor spreading". Geology, 10(7), 353–357.

Noack, V., Scheck-Wenderoth, M., Cacace, M., and Schneider, M. (2013). Influence of fluid flow on the regional thermal field: results from 3D numerical modelling for the area of Brandenburg (North German Basin). Environmental earth sciences, 70(8), 3523–3544.

Naeser, N. D., and McCulloh, T. H. (Eds.). (2012). Thermal History of Sedimentary Basins: Methods and Case Histories. Springer Science and Business Media.

Nürnberg, D., and Müller, R. D. (1991). The tectonic evolution of the South Atlantic from Late Jurassic to present. Tectonophysics, 191(1), 27–53.

O'Connor, J. M., and Duncan, R. A. (1990). Evolution of the Walvis Ridge-Rio Grande Rise Hot Spot System: Implications for African and South American Plate motions over plumes. Journal of Geophysical Research: Solid Earth, 95(B11), 17475–17502.

Pascal, C. (2015). Heat flow of Norway and its continental shelf. Marine and Petroleum Geology, 66, 956–969.

Pawlowski, R. (2008). The use of gravity anomaly data for offshore continental margin demarcation. The Leading Edge, 27(6), 722–727.

Rabinowitz, P. D., and LaBrecque, J. (1979). The Mesozoic South Atlantic Ocean and evolution of its continental margins. Journal of Geophysical Research: Solid Earth, 84(B11), 5973–6002.

Reiners, P. W., and Brandon, M. T. (2006). Using thermochronology to understand orogenic erosion. Annu. Rev. Earth Planet. Sci., 34, 419–466.

Ren, S., Skogseid, J., and Eldholm, O. (1998). Late Cretaceous-Paleocene extension on the Vøring volcanic margin. Marine Geophysical Researches, 20(4), 343–369.

Scheck-Wenderoth, M., Cacace, M., Maystrenko, Y. P., Cherubini, Y., Noack, V., Kaiser, B. O., ... and Björn, L. (2014). Models of heat transport in the Central European Basin System: Effective mechanisms at different scales. Marine and Petroleum Geology, 55, 315–331.

Scheck-Wenderoth, M., and Lamarche, J. (2005). Crustal memory and basin evolution in the Central European Basin System–new insights from a 3D structural model. Tectonophysics, 397(1), 143–165.

Scheck-Wenderoth, M., and Maystrenko, Y. (2008). How warm are passive continental margins? A 3-D lithosphere-scale study from the Norwegian margin. Geology, 36(5), 419–422.

Scheck-Wenderoth, M., Raum, T., Faleide, J. I., Mjelde, R., and Horsfield, B. (2007). The transition from the continent to the ocean: a deeper view on the Norwegian margin. Journal of the Geological Society, 164(4), 855–868.

Séranne, M., and Anka, Z. (2005). South Atlantic continental margins of Africa: a comparison of the tectonic vs climate interplay on the evolution of equatorial west Africa and SW Africa margins. Journal of African Earth Sciences, 43(1), 283–300.

Sippel, J., Scheck-Wenderoth, M., Lewerenz, B., and Klitzke, P. (2015). Deep vs. shallow controlling factors of the crustal thermal field-insights from 3D modelling of the Beaufort-Mackenzie Basin (Arctic Canada). Basin Research, 27(1), 102–123.

Skogseid, J. (1994). Dimensions of the late Cretaceous-Paleocene northeast Atlantic rift derived from Cenozoic subsidence. Tectonophysics, 240(1), 225–247.

Skogseid, J., Pedersen, T., Eldholm, O., and Larsen, B. T. (1992). Tectonism and magmatism during NE Atlantic continental break-up: the Vøring margin. Geological Society, London, Special Publications, 68(1), 305–320.

Skogseid, J., Planke, S., Faleide, J. I., Pedersen, T., Eldholm, O., and Neverdal, F. (2000). NE Atlantic continental rifting and volcanic margin formation. Geological Society, London, Special Publications, 167(1), 295–326.

Stewart, J., Watts, A. B., and Bagguley, J. G. (2000). Three-dimensional subsidence analysis and gravity modelling of the continental margin offshore Namibia. Geophysical Journal International, 141(3), 724–746.

Stockli, D. F., Farley, K. A., and Dumitru, T. A. (2000). Calibration of the apatite (U-Th)/He thermochronometer on an exhumed fault block, White Mountains, California. Geology, 28(11), 983–986.

Swiecicki, T., Gibbs, P. B., Farrow, G. E., and Coward, M. P. (1998). A tectonostratigraphic framework for the Mid-Norway region. Marine and Petroleum Geology, 15(3), 245–276.

Talwani, M., and Abreu, V. (2000). Inferences regarding initiation of oceanic crust formation from the US East Coast margin and conjugate South Atlantic margins. American geophysical Union.

Tissot, B. P., Pelet, R., and Ungerer, P. H. (1987). Thermal history of sedimentary basins, maturation indices, and kinetics of oil and gas generation. AAPG bulletin, 71(12), 1445–1466.

Tsikalas, F., Eldholm, O., and Faleide, J. I. (2002). Early Eocene sea floor spreading and continent-ocean boundary between Jan Mayen and Senja fracture zones in the Norwegian-Greenland Sea. Marine Geophysical Researches, 23(3), 247–270.

Turcotte, D. L., and Schubert, G. (2014). Geodynamics, Cambridge University Press.

Unternehr, P., Curie, D., Olivet, J. L., Goslin, J., and Beuzart, P. (1988). South Atlantic fits and intraplate boundaries in Africa and South America. Tectonophysics, 155(1-4), 169–179.

Wallmann, K., Pinero, E., Burwicz, E., Haeckel, M., Hensen, C., Dale, A., and Ruepke, L. (2012). The global inventory of methane hydrate in marine sediments: A theoretical approach. Energies, 5(7), 2449–2498.

White, R. S. (1989). Initiation of the Iceland Plume and Opening of the North Atlantic: Chapter 10: North Atlantic Perspectives.

White, R., and McKenzie, D. (1989). Magmatism at rift zones: the generation of volcanic continental margins and flood basalts. Journal of Geophysical Research: Solid Earth, 94(B6), 7685–7729.

White, R. S., Spence, G. D., Fowler, S. R., McKenzie, D. P., and Westbrook, G. K. (1987). Magmatism at rifted continental margins. Nature, 330, 439–444.